

Performance Improvement by Local Frequency Offset Spatial Diversity Reception with $\pi/4$ -DQPSK in Implant Body Area Networks

Daisuke ANZAI^{†a)}, Member, Takashi KOYA[†], Student Member, Jingjing SHI^{†b)}, Member, and Jianqing WANG^{†c)}, Fellow

SUMMARY Space diversity reception is well known as a technique that can improve the performance of wireless communication systems without any temporal and spectral resource expansion. Implant body area networks (BANs) require high-speed transmission and low energy consumption. Therefore, applying spatial diversity reception to implant BANs can be expected to fulfill these requirements. For this purpose, this paper presents a local frequency offset diversity system with $\pi/4$ -differential quadrature phase shift keying (DQPSK) for implant BANs that offer improved communication performance with a simpler receiver structure, and evaluates the proposal's bit error rate (BER) performance by theoretical analysis. In the theoretical analysis, it is difficult to analytically derive the probability density function (*pdf*) on the combined signal-to-noise power ratio (SNR) at the local offset frequency diversity receiver output. Therefore, this paper adopts the moment generating function approximation method and demonstrates that the resulting theoretical analyses yield performances that basically match the results of computer simulations. We first confirm that the local frequency offset diversity reception can effectively improve the communication performance of implant BANs. Next, we perform an analysis of a realistic communication performance, namely, a link budget analysis based on derived BER performance and evaluate the link parameters including system margin, maximum link distance and required transmit power. These analyses demonstrate that the local frequency offset diversity system can realize a reliable communication link in a realistic implant BAN scenario.

key words: local frequency offset diversity, $\pi/4$ -DQPSK, bit error rate, link budget

1. Introduction

With the miniaturization of electronic devices and the rapid growth of wireless communications, body area networks (BANs) have drawn considerable attention in healthcare and medical applications [1]–[3]. Generally, BANs are categorized into two groups: wearable BANs and implanted BANs. One of the applications of wearable BANs is medical monitoring, which can be used to monitor a person's healthy situation in daily life [2]. On the other hand, in implant BANs, capsule endoscopy has been one of the most important applications [5], [6]. Capsule endoscopy involves ingesting a small capsule, which contains a color camera, battery, light source and transmitter. The capsule endo-

scope takes pictures every second and transmits images to a data recorder in order to assist in diagnosing gastrointestinal conditions such as obscure gastrointestinal bleeding, mal-absorption, chronic abdominal pain and chronic diarrhoea. In this paper, we focus on the capsule endoscopy system, namely, implant BAN applications.

Since the capsule endoscope requires the establishment of reliable communication, it is essential to improve the transmission performance for the capsule endoscope. In order to improve the communication performance, introduction of diversity techniques into the receivers is effective. As a diversity reception technique, Maximal-ratio combining (MRC) and equal gain combining (EGC) are widely used. However, both are extremely complex since they require knowledge of the carrier phase of each signal or combine each signal after demodulation using parallel complete receiving systems. To simplify the spatial diversity schemes, local frequency offset diversity has been proposed [4]. The signal from each receiving branch is translated into a different intermediate frequency (IF), and then, the IF signals are combined without phase adjusters and detected by a common differential detector.

Furthermore, as the frequency band for the implant communications, the 400 MHz medical implant communication service (MICS) band is usually chosen. For example, a commercial available implant communication chip for cardiac pacemaker employs the 400 MHz band for data transmission [7]. However, the data rate is limited to several hundred kbps due to its narrow frequency band [8], [9]. In view of the implant communication application, for instance, the capsule endoscope needs a higher data rate for a real-time image and video transmission. So, bandwidth-efficient modulation is a key technology for wireless capsule endoscopy communication. To solve this problem, we pay attention to multilevel modulation schemes such as $\pi/4$ -differential quadrature phase shift keying (DQPSK), which can increase the data rate without expanding its frequency bandwidth. From the above reasons, this paper introduces a local frequency offset spatial diversity system with $\pi/4$ DQPSK into implant BAN applications and investigates the resulting improvement in communication performance.

When we evaluate the performance of the local frequency offset spatial diversity reception, the model of the propagation characteristics in the implant BANs at the

Manuscript received July 2, 2013.

Manuscript revised October 21, 2013.

[†]The authors are with Nagoya Institute Technology, Nagoya-shi, 466-8555 Japan.

a) E-mail: anzai@nitech.ac.jp

b) E-mail: shi.jingjing@nitech.ac.jp

c) E-mail: wang@nitech.ac.jp

DOI: 10.1587/transcom.E97.B.571

400 MHz MICS band is required. Therefore, this paper theoretically analyzes the bit error rate (BER) performance on the local frequency offset spatial diversity receiver with the propagation characteristics investigated by the finite-difference time-domain (FDTD) simulation. In place of the difficulty in actual measurement of propagation characteristics for living humans, FDTD simulation has a merit to provide high-quality propagation data by using an anatomically based high-resolution human body model [10]. In the theoretical analysis, it is difficult to derive the exact probability density function (*pdf*) on the combined E_b/N_0 at the spatial diversity receiver output. This is because that the joint *pdf* on E_b/N_0 at each diversity branch cannot be decomposed due to a correlation between the branches. Therefore, we introduce the moment generating function (MGF) approximation method [11], and the BER performances are analyzed by using the MGF approximation methods. Furthermore, in addition to the BER performance analysis, we perform a link budget analysis to investigate the link parameters including system margin, maximum link distance and required transmit power. Based on performance evaluation of the theoretical analyses and computer simulations, we confirm the performance improvement by the local frequency offset spatial diversity with $\pi/4$ -DQPSK in a realistic implant BANs scenario.

This paper is organized as follows. Section 2 presents the system model of the local frequency offset spatial diversity receiver. Section 3 describes the propagation characteristics in the implant BANs, and Sect. 4 denotes the theoretical analyses with the MGF approximation methods. Section 5 shows the BER performance and the results of the link budget analyses, and discusses them. Finally, Sect. 6 concludes this paper.

2. System Model of Local Frequency Offset Spatial Diversity Receiver

We assume a transmitter with a single antenna inside a human body and a diversity receiver with two antennas (branches) on the human body. In order to increase the data rate without expanding the frequency band, we assume a multilevel modulation scheme, so, in this paper, we employ $\pi/4$ -DQPSK (introducing further multilevel modulation schemes, i.e., 16 star QAM, is our future subject). Figure 1 shows the system model which is composed of a local frequency offset diversity receiver with two diversity branches. The receiver is equipped with two diversity branches, hence the wireless channel is decomposed into two fading sub-channels. Defining the received signal at the l -th diversity branch as $r_l(t)$ ($l = 1, 2$), $r_l(t)$ is given by

$$r_l(t) = \text{Re}[h_l(t) \otimes s(t) + n_l(t)] \quad (1)$$

where $s(t)$ is the transmitted signal. In (1), $h_l(t)$ and $n_l(t)$ denote the impulse response of the l -th sub-channel and the additive Gaussian noise at the l -th diversity branch, respectively, and \otimes denotes the convolution. Here, we assumed that $n_1(t)$ and $n_2(t)$ are independent with the same power.

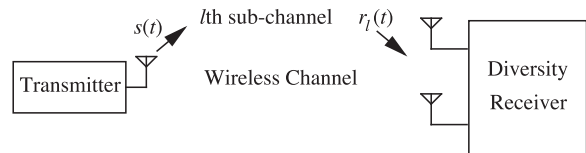


Fig. 1 System model.

Figure 2 shows a configuration of the local frequency offset diversity receiver with $\pi/4$ -DQPSK modulation. First, assuming flat fading channel environment, the received signal at each diversity branch $r_l(t)$ is given by

$$r_l(t) = \text{Re}[|h_l(t)|e^{j(2\pi f_c t + \phi(t) + \phi_l(t))} + n_l(t)] \quad (2)$$

where f_c , $\phi(t)$ and $\phi_l(t)$ represent the carrier frequency, the phase modulation component and the phase component of $h_l(t)$, respectively. The two local frequencies are offset from $f_c - f_i$ by δf , so the received signal at each branch $r_l(t)$ is translated to an IF stage with center frequencies of $f_i + \delta f$ and $f_i - \delta f$, that is, we obtain (for simple explanation, the noise component $n_l(t)$ is dropped)

$$r_1^{IF}(t) = \frac{1}{2}|h_1(t)| \cos[2\pi(f_i + \delta f)t + \phi(t) + \phi_1(t)] \quad (3)$$

$$r_2^{IF}(t) = \frac{1}{2}|h_2(t)| \cos[2\pi(f_i - \delta f)t + \phi(t) + \phi_2(t)] \quad (4)$$

where f_i and δf denote the IF frequency and the local offset frequency, respectively. After the IF frequency translation, we combine the two signals without phase adjusters, and the signals after sub-synchronization detector are represented as

$$X(t) = \frac{1}{4}|h_1(t)| \cos[2\pi\delta f t + \phi(t) + \phi_1(t)] + \frac{1}{4}|h_2(t)| \cos[2\pi\delta f t + \phi(t) + \phi_2(t)] \quad (5)$$

$$Y(t) = \frac{1}{4}|h_1(t)| \cos\left[2\pi\delta f t + \phi(t) + \phi_2(t) - \frac{\pi}{2}\right] + \frac{1}{4}|h_2(t)| \cos\left[-2\pi\delta f t + \phi(t) + \phi_2(t) - \frac{\pi}{2}\right]. \quad (6)$$

Then, the differential detector performs the following operations:

$$I(t) = X(t)X(t - T_s) + Y(t)Y(t - T_s) \quad (7)$$

$$Q(t) = Y(t)X(t - T_s) - X(t)Y(t - T_s) \quad (8)$$

where T_s is the symbol duration. Under the condition that $\delta f = n/(2T_s)$ (n :integer), after removing the high-frequency components of $2\delta f$ with the low pass filters (LPF2 in Fig. 2), we finally obtain the demodulated signals as

$$I_{low}(t) = \frac{1}{16} \left[|h_1(t)|^2 + |h_2(t)|^2 \right] \cos[\Delta\phi(t)] \quad (9)$$

$$Q_{low}(t) = \frac{1}{16} \left[|h_1(t)|^2 + |h_2(t)|^2 \right] \sin[\Delta\phi(t)]. \quad (10)$$

In the above equations, we assume a slow fading channel, namely, $\phi_l(t) = \phi_l(t + T_s)$ because the capsule endoscope (transmitter) moves the gastrointestinal tract with a quite

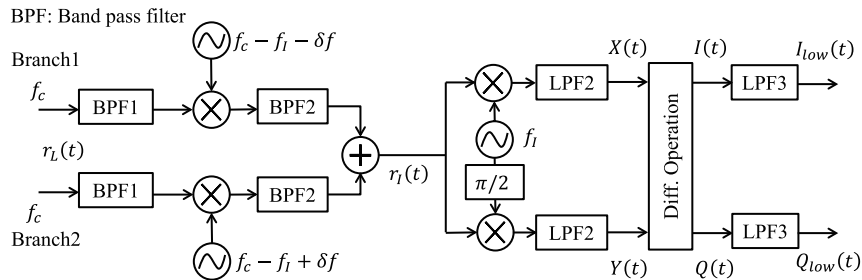


Fig. 2 Configuration of local frequency offset spatial diversity receiver.

slow speed. Here, we would like to again emphasize that the local frequency offset diversity receiver requires no phase adjuster, which leads to the increase of computational complexity and energy consumption at the receiver side, and the phase adjuster is essential for MRC and EGC spatial diversity systems. Furthermore, from (9) and (10), we can see that the signal-to-noise power ratio (SNR) of combined output is perfectly corresponding to that of EGC combiner, which is obtained as

$$SNR^{output} = \frac{(\sum_{l=1}^2 |h_l(t)|)^2}{\sum_{l=1}^2 N_l} \quad (11)$$

where N_l is the power of the additive white Gaussian noise at the l -th branch.

3. Propagation Characteristics

3.1 Path Loss and Shadow Fading Characteristics

To analyze propagation characteristics, we employed FDTD simulation with a numerical human body model, which was developed by National Institute of Information and Communication Technology, Japan [12]. The human body model is 1.73 m tall and 65 kg weight, and is composed of 51 kinds of biological tissues with a spatial resolution of 2 mm. A 4-mm long dipole as the transmit antenna of a WCE was moved to have 30 locations with three directivities inside the human body, and five receive antennas, denoted as in Fig. 3 with Rx_i ($i = 0, 1, \dots, 4$), were 20-mm long dipoles fixed in front of the body.

From [13], the average path loss $PL_{dB}^{average}$ can be expressed as

$$PL_{dB}^{average} = PL_{0,dB} + 10n \log_{10} \frac{d}{d_0} \quad (12)$$

where d_0 , $PL_{0,dB}$ and n are a reference distance, the path loss at the reference distance d_0 and the path loss exponent, respectively. The parameters in (12) fitted to the FDTD simulation results are shown in Table 1.

Additionally, we consider shadow fading characteristics from the implant BAN channel. Defining S as $PL/PL^{average}$, the pdf on S is given by [13]

$$p(S) = \frac{1}{\sqrt{2\pi\sigma^2 S}} \exp\left[-\frac{(\log S - \mu)^2}{2\sigma^2}\right] \quad (13)$$

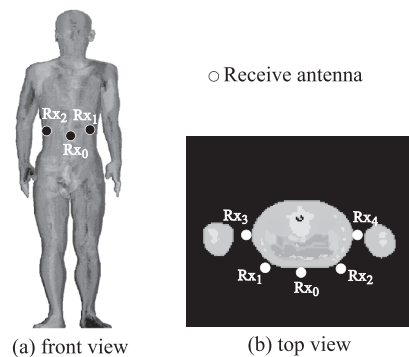


Fig. 3 Positions of receive antennas.

Table 1 Fitted parameters of propagation characteristics.

	d_0 [m]	$PL_{0,dB}$	n	μ	σ
Rx0	0.05	49.67	5.533	0	2.04
Rx1	0.05	37.99	6.663	0	1.80
Rx2	0.05	37.81	5.997	0	2.20
Rx3	0.1	59.74	6.421	0	2.17
Rx4	0.1	58.62	5.793	0	2.17

where μ and σ denote the mean and the standard deviation in log domain, respectively, which are also summarized in Table 1.

3.2 Correlation Coefficient

Finally, we demonstrate correlation coefficients between received signals of two branches. Let us define the correlation coefficient between the two received signals of Rx_l and Rx_k ($l, k = 0, 1, \dots, 4$) as

$$\rho_{l,k} = \frac{E[(r_l(t) - m_l)(r_k(t) - m_k)]}{\sqrt{E[(r_l(t) - m_l)^2]} \sqrt{E[(r_k(t) - m_k)^2]}} \quad (14)$$

$$m_l = E[r_l(t)] \quad (15)$$

where $r_l(t)$ and $E(\cdot)$ are the received signal at the l -th branch defined by (1) and the ensemble average of (\cdot) , respectively. In Table 2, we summarize the correlation coefficients $\rho_{l,k}$ based on the FDTD-simulated results. From this table, it is observed that the correlation coefficients range from 0.076 to 0.821, which suggests the feasibility of space diversity reception.

Table 2 Correlation coefficients between two received signals.

	Rx ₀	Rx ₁	Rx ₂	Rx ₃	Rx ₄
Rx ₀	–				
Rx ₁	0.306	–			
Rx ₂	0.399	0.692	–		
Rx ₃	0.076	0.594	0.209	–	
Rx ₄	0.399	0.524	0.821	0.219	–

4. Theoretical Analysis

4.1 Single Branch

Before deriving a theoretical analysis of the BER performance for the local frequency offset spatial diversity, we explain the BER performance of the single branch case at first. The average BER for the single branch case is calculated as

$$P_b^{single}(\bar{\gamma}) = \int_0^\infty P_b^{AWGN}(\gamma) p(\gamma|\bar{\gamma}) d\gamma \quad (16)$$

where $\bar{\gamma}$, $P_b^{AWGN}(\gamma)$ and $p(\gamma|\bar{\gamma})$ are the average E_b/N_0 , the average BER under additive white Gaussian noise (AWGN) when the E_b/N_0 is γ and the *pdf* on the E_b/N_0 γ when $\bar{\gamma}$ is given, respectively. Taking into consideration that S is lognormally distributed as shown in (13), $p(\gamma|\bar{\gamma})$ can be derived as

$$p(\gamma|\bar{\gamma}) = \frac{1}{\sqrt{2\pi}\sigma\gamma} \exp\left[-\frac{(\log \gamma - \log \bar{\gamma})^2}{2\sigma^2}\right]. \quad (17)$$

Now, assuming the $\pi/4$ -DQPSK modulation, $P_b^{AWGN}(\gamma)$ is calculated as [14]

$$P_b^{AWGN}(\gamma) = \frac{1}{2} [1 - Q(\sqrt{b}, \sqrt{a}) + Q(\sqrt{a}, \sqrt{b})] \quad (18)$$

where

$$a = (2 - \sqrt{2})\gamma, \quad b = (2 + \sqrt{2})\gamma. \quad (19)$$

In (18), $Q(a, b)$ is the Marcum Q-function, which is defined as

$$Q(a, b) = \int_b^\infty x \exp\left(-\frac{x^2 + a^2}{2}\right) I_0(ax) dx. \quad (20)$$

4.2 Spatial Diversity with Multiple Branches

We theoretically analyze BER performance for the local frequency offset spatial diversity receiver. Assuming the average E_b/N_0 at each branch $\bar{\gamma}_l$ ($l = 1, 2$) is the same as each other, the average BER for the local frequency offset diversity receiver is given by

$$P_b^{diversity}(\bar{\gamma}) = \int_0^\infty P_b^{AWGN}(\gamma_o) p(\gamma_o|\bar{\gamma}) d\gamma_o \quad (21)$$

where γ_o means the E_b/N_0 of the combined output at the local frequency offset diversity system. SNR_{output} is represented by (11), and as a result, γ_o includes the sum of two

correlated lognormally distributed random variables ($|h_l(t)|$ in (11) is lognormally distributed). Since it is difficult to derive exact closed-form expressions for the *pdf*, we can approximate the *pdf* on γ_o with the moment generating function (MGF) approximation method [11]. Note that, the MGF approximated *pdf* on γ_o is represented as a lognormal distribution because the *pdf* on the lognormal sum is well approximated by the lognormal distribution. So, the MGF approximation method estimates the parameters σ and μ of the lognormal distribution.

4.3 Moment Generating Function Approximation Method for Correlated Lognormal Sum

The MGF of a lognormal random variable X can be written as

$$\begin{aligned} \Psi_X(s) &= \int_0^\infty \exp(-sx) p_X(x) dx, \quad (\text{Re}(s) \geq 0) \\ &= \int_0^\infty \frac{\xi \exp(-sx)}{x\sigma\sqrt{2\pi}} \exp\left[-\frac{(\xi \log x - \mu)^2}{2\sigma^2}\right] dx \\ &= \sum_{n=1}^N \frac{w_n}{\sqrt{\pi}} \exp\left[-s \exp\left(\frac{\sqrt{2}\sigma a_n + \mu}{\xi}\right)\right] + R_N \end{aligned} \quad (22)$$

where ξ , N and R_N are a scaling constant (in this case, $\xi = 10 \log_e 10$), the Hermite integration order and a remainder term, respectively. Here, the weights w_n and the abscissas a_n can be found in [15]. From (22), by removing R_N , this paper defines the Gauss-Hermite representation of the MGF $\hat{\Psi}$ as

$$\hat{\Psi}_X(s; \mu, \sigma) = \sum_{n=1}^N \frac{w_n}{\sqrt{\pi}} \exp\left[-s \exp\left(\frac{\sqrt{2}\sigma a_n + \mu}{\xi}\right)\right]. \quad (23)$$

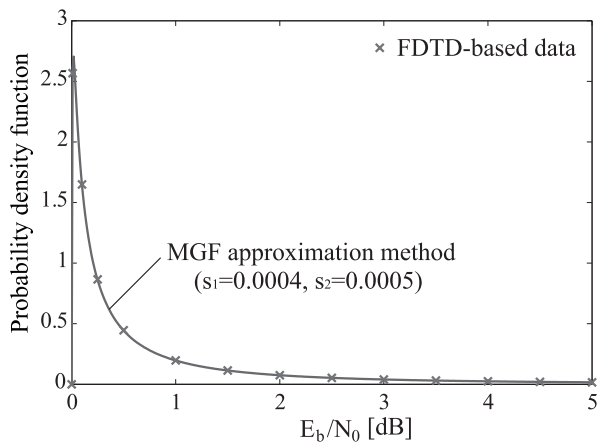
The MGF approximation method finds the parameters of the correlated lognormal sum as follows:

$$\begin{aligned} &\text{find } \sigma \text{ and } \mu \text{ which satisfy} \\ &\hat{\Psi}_X(\mathbf{s}_m; \mu, \sigma) \\ &= \sum_{n_1=1}^N \sum_{n_2=1}^N \frac{w_{n_1} w_{n_2}}{\pi} \\ &\quad \times \exp\left\{-\mathbf{s}_m \left[\exp\left(\frac{\sqrt{2}\sigma_1 a_{n_1} + \mu_1}{\xi}\right) \right. \right. \\ &\quad \left. \left. + \exp\left(\frac{\sqrt{2}\rho\sigma_2 a_{n_1} + \sqrt{2}(1-\rho^2)\sigma_2 a_{n_2} + \mu_2}{\xi}\right) \right]\right\} \\ &\text{for } m = 1 \text{ and } 2 \end{aligned} \quad (24)$$

where we determine $N = 6$, $\mathbf{s}_1 = 0.0004$ and $\mathbf{s}_2 = 0.0005$ in this paper. These parameters are optimized by a greedy algorithm in a preliminary simulation [16]. In (24), μ_i and σ_i ($i = 1, 2$) are the parameters of the shadow fading characteristics for each branch.

Table 3 Computer simulation parameters.

Carrier frequency f_c	400 MHz
Data rate f_b	2 Mbps
Local offset frequency δf	2 MHz
IF frequency f_i	10 MHz
Cutoff frequency of LPF1 in Fig. 2	10 MHz
Cutoff frequency of LPF2 in Fig. 2	1.2 MHz
Transmitter output power	20 mW
Standard temperature T_0	300 K
Boltzmann constant k	1.38×10^{-23} J/K
Receiver noise figure $N_{F,dB}$	6 dB
Thermal noise power spectrum $N_{0,dB}$	-198 dBW/Hz

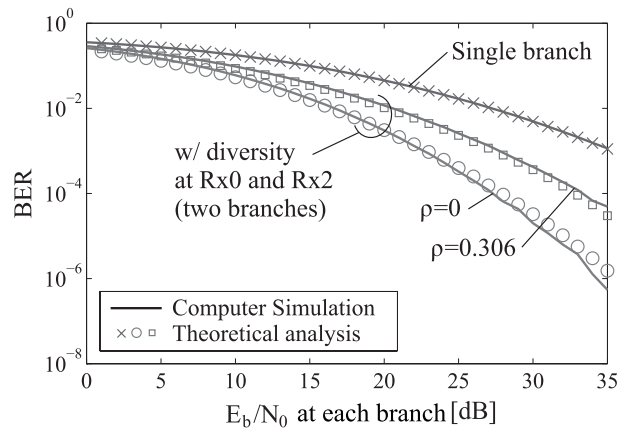
**Fig. 4** Approximation of the pdf on E_b/N_0 of combined output.

5. Performance Evaluations and Discussions

5.1 BER Performance

We calculate the parameters of the $p(\gamma_{EGC})$ by the approximation method before evaluating the BER performance for the local frequency offset diversity receiver. In this section, we put two branches at the location of Rx_0 and Rx_2 , that is, we choose the parameters of Rx_0 and Rx_2 tabulated in Table 1 (the results for the other selection of the receivers are similar to that for the selection of Rx_0 and Rx_2 , so they are omitted in this paper). Table 3 summarizes the parameters of the computer simulations. The setting of larger frequency bandwidth and transmitter output power compared to the MICS regulation is just for demonstrate the possibility of high-speed transmission. Figure 4 shows the pdf s on the E_b/N_0 of the combined output approximated by the MGF methods. Also, Fig. 4 includes the pdf obtained from the FDTD-based data. From this figure, we can see that the MGF approximation method is close to the FDTD-based data. Here, we would like to note that the MGF approximation requires only information of the parameters on the log-normal distribution, namely, μ and σ of Rx_0 and Rx_2 and the correlation coefficient between Rx_0 and Rx_2 ρ in this case.

Figure 5 shows the average BER for the local frequency offset diversity receiver by the theoretical analyses with the results of the MGF approximation method against the E_b/N_0

**Fig. 5** BER performances of theoretical analyses and computer simulations.

at each branch. For comparison purpose, Fig. 5 also shows the average BER for the local frequency offset diversity receiver by a computer simulation, where the computer simulation parameters are the same as those of the theoretical analysis. From this figure, we observe good agreements between the results of the theoretical analyses and the computer simulation. Furthermore, Fig. 5 also shows the average BER for the case of a single branch at Rx_0 by the theoretical analysis and the computer simulation. As compared with the case of a single branch, the local frequency offset diversity with two branches can improve the BER performance effectively. Moreover, to investigate the impact of the correlation coefficient ρ on the BER performance, we choose the correlation coefficient of $\rho = 0$ (perfectly uncorrelated) in addition to $\rho = 0.306$ (the correlation coefficient between Rx_0 and Rx_2). As can be seen from this figure, the BER performance is inversely proportional to the correlation coefficient, so it is important to select receive antennas (branches) with as little correlation as possible. However, in the case of the actual correlation coefficient $\rho = 0.306$, the performance improvement is around 5 dB at $BER = 10^{-3}$, as compared with the performance for the single branch. Moreover, if we optimally choose the two branches with an almost uncorrelated correlation coefficient ($\rho \approx 0$), the performance can be significantly improved by around 10 dB.

5.2 System Margin

Then, we perform an analysis of a realistic communication performance, namely, a link budget analysis based on derived BER performance and evaluate the link parameters including system margin, maximum link distance and required transmit power. For the link budget analysis, we first define the system margin M_s as

$$M_s = \frac{E_b/N_0}{[E_b/N_0]_{spec}} \quad (25)$$

where $[E_b/N_0]_{spec}$ denotes the required E_b/N_0 for obtaining a specific BER. In (25), if the link E_b/N_0 exceeds the required $[E_b/N_0]_{spec}$, which means system margin $M_s \geq 0$ dB,

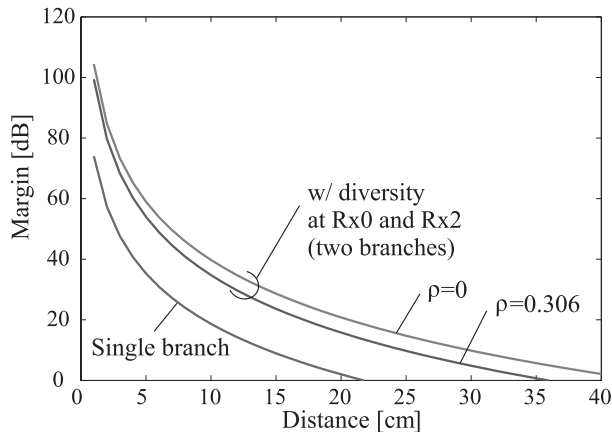


Fig. 6 Dependence of system margin on distance.

the wireless communication is feasible. The larger the system margin is, the more reliable and robust the communication is. In this paper, we use the BER of 10^{-3} because such a BER performance means that it is possible to obtain an error-free BER ($< 10^{-10}$) if we adapt an adequate forward error correction code [17]. From the BER performance as shown in Fig. 5, we can obtain the required E_b/N_0 as the BER performance of 10^{-3} .

The received power can be expressed by using the path loss model represented in (12) under the maximum transmit power as

$$\begin{aligned} P_{r,dBW} &= P_{t,dBW} - PL_{dB} \\ &= P_{t,dBW} - PL_{0,dB} - 10n \log_{10}(d/d_0). \end{aligned} \quad (26)$$

In (26), we note that the transmit and receive antenna gains are assumed as 0 dBi, and the other losses are assumed as 0 dB. As for the maximum transmit power, according to the ICNIRP guideline [18], a local specific absorption rate (SAR) as averaged over any ten grams of human tissue should never exceed 2 W/kg (or 10 W/kg for occupational people). In this sense, 20 mW or 13 dBm may be acceptable since such a transmit power can never induce a 10-gram average SAR exceeding 2 W/kg. From the above reasons, we set the maximum transmit power to 20 mW. Consequently, by using (26), E_b/N_0 can be obtained as

$$E_b/N_{0,dB} = P_{r,dBW} - 10 \log_{10} f_b - N_{0,dB} \quad (27)$$

where f_b is the data rate, and $N_{0,dB}$ is the thermal noise power spectrum density, which is given by

$$N_{0,dB} = 10 \log_{10}(kT_0) + N_{F,dB} \quad (28)$$

where T_0 , k and $N_{F,dB}$ denote the environment temperature, the Boltzmann constant, and the noise figure of the receiver front-end, respectively. Table 3 also includes these parameters. It should be noted that the only noise source at the receiver is AWGN in (28).

Figure 6 shows the dependence of system margin M_s on link distance. As can be seen from Fig. 6, the system margin of the local frequency offset diversity reception can

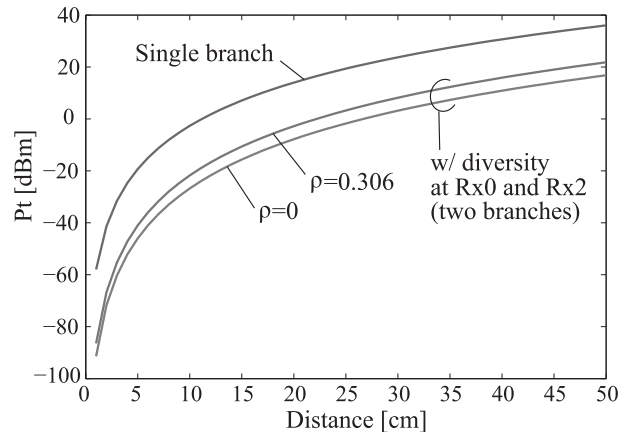


Fig. 7 Required transmit power versus link distance.

be significantly improved as compared with that of the single branch. For example, at the system margin of 20 dB, the local frequency offset diversity system accomplish the link distance of around 20 cm even if the correlation coefficient ($\rho = 0.306$) exists. On the other hand, the link distance for the single branch is only 10 cm at most. This result means that the local frequency offset diversity receiver can establish reliable communication (the BER = 10^{-3}) up to 20 cm with the system margin of 20 dB.

5.3 Required Transmit Power

Finally, let us discuss the required transmit power. The required transmit power can be calculated from (26) and (27) as

$$\begin{aligned} P_{t,dBW} &= E_b/N_{0,dB} + N_{0,dB} + 10 \log_{10} f_b + PL_{0,dB} \\ &\quad + 10n \log_{10}(d/d_0) \end{aligned} \quad (29)$$

where the E_b/N_0 is set to $[E_b/N_0]_{spec}$ to obtain the BER performance of 10^{-3} .

Figure 7 shows the required transmit power as a function of link distance. In addition to the improvement of the BER performance and the system margin, we can see from Fig. 7 that the introduction of the local frequency offset diversity receiver can extremely reduce the required transmit power. For instance, when the communication distance is 10 cm, as compared between the two results for the local frequency offset diversity with two branches and the single branch, the reduction of the required transmit power is around 20 dB. Furthermore, according to the MICS band regulation or IEEE 802.15.6 standard [19], the maximum emission power should be below $25 \mu\text{W}$ or -16 dBm . Even if the maximum transmit power is limited to such a low transmit power, the local frequency offset diversity receiver can still extend the link distance to around 15 cm inside the human body at a data rate of 2 Mbps, whereas the achievable link distance for the single branch is only 5 cm.

6. Conclusions

In this paper, we introduced the local frequency offset spatial diversity system with $\pi/4$ -DQPSK in order to realize reliable implant BAN communication without expanding the frequency bandwidth. Local frequency offset diversity provides the same performance as EGC diversity via a simpler receiver structure. To evaluate performance of the local frequency offset diversity receiver, to begin with, we theoretically analyzed the BER performance in the case of the correlated diversity branches with the MGF approximation method. Our theoretical analyses of the BER performance are almost corresponding to the result of the computer simulations even if the two diversity branches are correlated with each other. From the BER performance analysis, we have confirmed that the local frequency offset diversity with two branches is effective to improve the BER performance.

Furthermore, in addition to the BER performance evaluation, we performed a link budget analysis including the system margin and the required transmit power. Based on the analyses, we have concluded that the local frequency offset diversity receiver can establish reliable communication (the BER = 10^{-3}) up to 20 cm with a system margin of 20 dB. Taking the MICS band regulation or IEEE 802.15.6 standard into consideration, our spatial diversity system is able to extend the link distance to around 15 cm at 2 Mbps, whereas the achievable link distance for the single branch is only 5 cm. It should be noted that if we choose a different carrier frequency for the transmitting signals, although the path loss characteristics and the data rate will be consequently changed, the BER performance and the link budget can be still obtained by the same analysis procedure of this paper.

A future subject is to apply multilevel modulation, such as 16 star QAM, to the local frequency offset diversity receiver, and investigate its impact on the communication performance for implant BAN applications.

Acknowledgement

This study was supported in part by the Support Center for Advanced Telecommunications Technology Research (SCAT).

References

- [1] H.B. Li and R. Kohno, "Body area network and its standardization at IEEE 802.15. BAN," *Advances in Mobile and Wireless Communications*, pp.223–238, Springer, 2008.
- [2] E. Monton, J.F. Hernandez, J.M. Blasco, T. Herve, J. Micallef, I. Grech, A. Brincat, and V. Traver, "Body area network for wireless patient monitoring," *IET Communications*, vol.2, no.2, pp.215–222, Feb. 2008.
- [3] J. Wang and Q. Wang, *Body Area Communications*, Wiley, 2013.
- [4] J. Wang and T. Takagi, "Performance of local frequency offset space diversity for 16 star QAM," *IEEE Electron. Lett.*, vol.30, no.19, pp.1578–1579, Sept. 1994.
- [5] G. Iddan, G. Meron, A. Glukhovsky, and P. Swain, "Wireless capsule endoscopy," *Nature*, vol.405, p.417, May 2000.
- [6] G. Costamagna, S.K. Shah, M.E. Riccioni, F. Foschia, M. Mutignani, V. Perri, A. Vecchioli, M.G. Brizi, A. Picciocchi, and P. Marano, "A prospective trial comparing small bowel radiographs and video capsule endoscopy for suspected small bowel disease," *Gastroenterology*, vol.123, no.4, pp.999–1005, Oct. 2002.
- [7] Microsemi Corporation URL: <http://www.microsemi.com>
- [8] M.R. Yuce and T. Dissanayake, "Easy-to-swallow wireless telemetry," *IEEE Microw. Mag.*, vol.13, no.6, pp.90–101, Sept. 2012.
- [9] M.R. Yuce, T. Dissanayake, and H.C. Keong, "Wireless telemetry for electronic pill technology," *IEEE Sensors*, pp.1433–1438, Oct. 2009.
- [10] Q. Wang, T. Tayamachi, I. Kimura, and J. Wang, "An on-body channel model for UWB body area communications for various postures," *IEEE Trans. Antennas Propag.*, vol.57, no.4, pp.991–998, April 2009.
- [11] N.B. Mehta, J. Wu, A.F. Molisch, and J. Zhang, "Approximating a Sum of Random Variables with a Lognormal," *IEEE Trans. Wireless Commun.*, vol.6, no.7, pp.2690–2699, July 2007.
- [12] T. Nagaoka, S. Watanabe, K. Sakurai, E. Kunieda, S. Watanabe, M. Taki, and Y. Yamanaka, "Development of realistic high-resolution whole-body voxel models of Japanese adult males and females of average height and weight, and application of models to radio-frequency electromagnetic-field dosimetry," *Phys. Med. Biol.*, vol.49, pp.1–15, Jan. 2004.
- [13] D. Anzai, S. Aoyama, M. Yamanaka, and J. Wang, "Impact of spatial diversity reception on SAR reduction in implant body area networks," *IEICE Trans. Commun.*, vol.E95-B, no.12, pp.3822–3829, Dec. 2012.
- [14] M.K. Simon and M.S. Alouini, *Digital Communication over Fading Channels*, Wiley, 2004.
- [15] M. Abramowitz and I. Stegun, *Handbook of mathematical functions with formulas graphs, and mathematical tables*, 9th, Dover, 1972.
- [16] J. Shi, D. Anzai, and J. Wang, "UWB diversity performance in correlated lognormal-sum-distributed in-body to on-body channel," *IEICE Commun. Express*, vol.1, no.5, pp.171–176, Oct. 2012.
- [17] R. Mehmood, E. Cerqueira, R. Piesiewicz, and I. Chlamtac, *Communications Infrastructure, Systems and Applications*, Springer-Verlag New York, 2010.
- [18] ICNIRP, "Guidelines for limiting exposure to time-varying electric, magnetic and electromagnetic fields (up to 300 GHz)," *Health Physics*, vol.74, pp.494–522, 1998.
- [19] IEEE Standard for local and metropolitan area networks—Part 15.6: Wireless Body Area Networks, Feb. 2012.



Daisuke Anzai received the B.E., M.E. and Ph.D. degrees from Osaka City University, Osaka, Japan in 2006, 2008 and 2011, respectively. Since April 2011, he has been an Assistant Professor at the Graduate School of Engineering, Nagoya Institute of Technology, Nagoya, Japan. He has engaged in the research of biomedical communication systems and localization systems in wireless communication networks.



Takashi Koya was born in Gifu, Japan, in 1990. He received the B.Eng. degree from Nagoya Institute of Technology, Aichi, Japan in 2013. He is currently pursuing the M.Eng. course at Nagoya Institute of Technology, engaging in the research on wireless communication in body area networks.



Jingjing Shi received the B.E. degree from Shenyang University of Chemical Technology, Shenyang, China, in 2007, and the M.E. and D.E. degree from Nagoya Institute of Technology, Nagoya, Japan, in 2010 and 2013, respectively. She is currently at Nagoya Institute of Technology as a Postdoctoral Research Associate. Her research interests involve biomedical communications in wireless communication networks.



Jianqing Wang received the B.E. degree in electronic engineering from Beijing Institute of Technology, Beijing, China, in 1984, and the M.E. and D.E. degrees in electrical and communication engineering from Tohoku University, Sendai, Japan, in 1988 and 1991, respectively. He was a Research Associate at Tohoku University and a Senior Engineer at Sophia Systems Co., Ltd., prior to joining the Nagoya Institute of Technology, Nagoya, Japan, in 1997, where he is currently a Professor. His research interests include biomedical communications and electromagnetic compatibility.